Spin liquid fingerprints in the thermal transport of a Kitaev-Heisenberg ladder

Alexandros Metavitsiadis, Christina Psaroudaki, and Wolfram Brenig

Phys. Rev. B **99**, 205129 — Published 17 May 2019

DOI: 10.1103/PhysRevB.99.205129

Spin liquid fingerprints in the thermal transport of a Kitaev-Heisenberg ladder

Alexandros Metavitsiadis,[1,*] Christina Psaroudaki,[2,†] and Wolfram Brenig[1,‡]

[1] *Institute for Theoretical Physics, Technical University Braunschweig, D-38106 Braunschweig, Germany*
[2] *Department of Physics, University of Basel, Klingelbergstrasse 82, 4056 Basel, Switzerland*

(Dated: April 10, 2019)

We identify fingerprints of a proximate quantum spin-liquid (QSL), observable by finite-temperature dynamical thermal transport within a minimal version of the idealized Kitaev model on a two-leg ladder, if subjected to inevitably present Heisenberg couplings. Using exact diagonalization and quantum typicality, we uncover (i) an insulator-conductor crossover induced by recombination of fractionalized excitations at small Heisenberg couplings, (ii) low- and high-energy signatures of fractionalized excitations, which survive far off the pure QSL point, and (iii) a non-monotonous current life-time versus Heisenberg couplings. Guided by perturbation theory, we find (iv) a Kitaev-exchange induced "one-magnon" contribution to the dynamical heat transport in the strong Heisenberg rung limit.

I. INTRODUCTION

A quantum spin liquid (QSL) is an elusive state of magnetic matter with the intriguing property of lacking a local magnetic order parameter in the absence of external fields at any temperature T[1,2]. Instead, QSLs may show quantum orders, massive entanglement and exotic fractional elementary excitations, e.g. spinons[3–5], Majorana fermions, gauge vortices[6,7] and alike. QSLs are a consequence of frustrating exchange couplings, such that the local magnetic moments cannot simultaneously satisfy their mutual interactions[8]. In a seminal paper[9], Kitaev introduced an exactly solvable $\mathbb{Z}_2$ QSL-model, where spin-1/2 operators reside on the vertices of a honeycomb lattice and are subject to exchange frustration from Ising interactions of the type XX, YY, or ZZ depending on the direction of the bond[10]. Early on, it was proposed that such patterns can be realized in optical lattices[11], and shortly after also in Mott-Hubbard insulators with strong spin orbit coupling[12,13]. In the quest for materials which host Kitaev physics, several compounds have surfaced, e.g. the iridates α-Na_2IrO_3 or α-Li_2IrO_3, as well as α-$RuCl_3$. The latter systems, however, all order magnetically at low temperatures due to additional interactions[14–17]. Recently, $H_3LiIr_2O_6$ has been synthesized, which reportedly shows no magnetic order at temperatures $\gtrsim 10^{-4}J$, with J the exchange interaction[18].

Low-T magnetic ordering is the common obstacle in real materials, preempting the putative formation of a QSL. Therefore, it is of tantamount importance to identify and interpret fingerprints, genuine to a QSL in systems which are subject to residual interactions obscuring the QSL behavior. For Kitaev magnets, this is not trivial and largely under debate[19–24]. In this endeavor, thermal transport has also been employed. Unlike to other magnetic systems[25,26], the longitudinal thermal conductivity κ_{xx} in α-$RuCl_3$ is predominantly phononic with, however, some hints of magnetic contributions[27–31]. Whether this is due to remnants of Majorana fermions due to the underlying Kitaev interactions, is not clear. Stronger evidence of Kitaev physics might show up in finite external magnetic fields (not considered here), because the low temperature magnetic order is suppressed[32] and it could give rise to a quantized thermal Hall conductance[33].

Theoretically, thermal transport studies in pure Kitaev QSLs have been performed via quantum Monte Carlo simulations in 2D[34] or via exact diagonalization (ED) in 1D and 2D[35,36]. Moment expansions might also provide high-temperature analytic results for thermal transport of pure Kitaev QSLs in the future[37]. Thermal transport was also studied in magnetically *ordered* phases of a Kitaev-Heisenberg model using spin wave calculations[38]. However, the impact of isotropic Heisenberg exchange on thermal transport, perturbing a pure Kitaev QSL, is a completely open issue. Here our work makes a step forward. We study the thermal transport properties of a Kitaev-Heisenberg ladder, using ED, dynamical quantum typicality (DQT), and perturbation theory. By tuning the exchange couplings between the limits of a pure Kitaev ladder (KL) and a Heisenberg ladder (HL), we provide a comprehensive view on the transport properties, while crossing over from a $\mathbb{Z}_2$ QSL into a conventional valence bond state with gapped triplon excitations. En route, we emphasize characteristics which serve to identify signatures of Kitaev physics at moderate Heisenberg couplings, describing a proximate QSL[39,40].

II. MODEL

The Hamiltonian for the Kitaev-Heisenberg model on a ladder of L rungs with boundary conditions is given by

$$H = \sum_{a=x,y,z} \sum_{\langle i,j \rangle} J^a_{ij} S^a_i S^a_j + J_{ij} S^a_i S^a_j \ . \tag{1}$$

Here S are spin-1/2 operators, and the restricted sum over i,j reproduces the geometry depicted in Fig. 1. $J^a_{ij} = J_x, J_y, J_z$ denote the anisotropic Kitaev interactions–only one of them is non-zero per bond–which we parametrize in terms of the coupling strength J_K. On the other hand, $J_{ij} = J_H, J'_H$ are SU(2) invariant Heisenberg interactions. If $J_H \neq J'_H$ is considered we will note

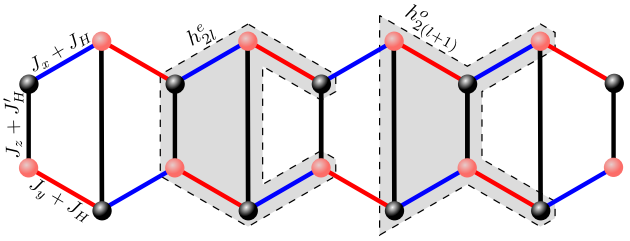

FIG. 1. The Kitaev-Heisenberg ladder. J_x, J_y, and J_z denote Ising interactions, while J_H and J'_H SU(2) invariant Heisenberg interactions. The local energy densities h^e_l and h^o_l used to define the energy current are highlighted.

this explicitly. Lastly, we set the lattice constant equal to unity, as well as the Planck and Boltzmann constants.

In the absence of Heisenberg interactions ($J_{ij} = 0$) the system is a $\mathbb{Z}_2$ spin liquid[7,41,42]. The spin degrees of freedom fractionalize into two species of Majorana fermions and the Hamiltonian acquires the form[7]

$$H = -\frac{i}{4}\sum_b J_x c_b c_r + J_y c_b c_r - J_z(i\bar{c}_b\bar{c}_r)c_b c_r\,. \qquad (2)$$

Here $c, \bar{c}$ represent Majorana fermions, $\{c_i, c_j\} = 2\delta_{ij} = \{\bar{c}_i, \bar{c}_j\}$, while the indices b and r correspond to the "black" and "red" sites of the lattice respectively. The quantity in the parenthesis is a good quantum number of the model, $\eta = i\bar{c}_b\bar{c}_r = \pm 1$, and therefore the $\bar{c}$ species becomes static. By defining Dirac fermions from pairs of Majorana fermions residing on the two sites of the same rung, Hamiltonian (2) transforms to a tight-binding *chain* with pairing terms in the presence of a $\mathbb{Z}_2$ gauge field. The latter acts as a disorder potential. The ground state of the system lies in the uniform η-sectors, and it can either be gapless for $|J_x - J_y| = J_z$, or gapped otherwise.

The transport properties of the quasi-1D KL were analyzed in Ref. [35]. It was shown, that the sole carriers of heat, the Majorana fermions, scatter from the thermally activated static gauge disorder such, that localization occurs. I.e. the KL turns into an ideal heat insulator at all temperatures. In the pure 2D Kitaev model similar scattering occurs, but too weak to force localization, leading to normal heat conduction[34,36]. In contrast, the HL exhibits a ground state continuously connected to a rung-singlet product (RSP) state, and triplon excitations[43]. The energy transport of the HL has been analyzed exhaustively over wide ranges of coupling strengths and temperatures and is well understood to be diffusive[44,45].

To analyze the thermal transport properties of our system, we obtain the energy current operator j^ϵ from the time derivative of the polarization operator, $P^\epsilon = \sum_l 2l h_{2l}$[46], which yields $j^\epsilon = -2i\sum_l [h_{2l}, h_{2(l-1)}]$. Here, we choose $h_{2l} = (h^e_{2l} + h^o_{2l})/2$, see Fig. 1. The real part of the energy current correlation function is given by $C(t) = \mathrm{Re}[\langle j^\epsilon(t) j^\epsilon\rangle/L]$, where the brackets $\langle\cdots\rangle$ denote the thermal mean value at temperature T. The thermal Drude weight D as well as the regular part κ' of the thermal conductivity, $\kappa(\omega) = 2\pi D\delta(\omega) + \kappa'(\omega)$, are obtained via

$$D = \frac{\beta^2}{2}C_0,\ \kappa'(\omega) = \mathcal{P}\frac{2\beta}{\omega}\tanh\frac{\beta\omega}{2}\int_0^\infty dt\cos\omega t\, C(t). \quad (3)$$

Here, $\beta = 1/T$, $\mathcal{P}$ the principal value, and C_0 the time independent contribution of degenerate states to $C(t)$. The static value of the regular part is determined by the limiting procedure $\kappa_{dc} = \kappa'(\omega \to 0)$. A finite value of D signifies dissipationless energy transport, whereas the contribution of dissipative modes to the normal dc conductivity is obtained by κ_{dc}. In the case where D and κ_{dc} vanish simultaneously the system is an ideal heat insulator[47].

The thermal mean values are calculated numerically either using ED by tracing over the full Hilbert space, or by using DQT which is expected to work well for high-dimensional Hilbert spaces and at not too low temperatures. In DQT, the thermal mean value is approximated by an expectation value obtained from a single pure random state $|\psi\rangle$, drawn from a distribution that is invariant under all unitary transformations in Hilbert space (Haar measure), and evolved to $|\psi_\beta\rangle = e^{-\beta H/2}|\psi\rangle$ to account for finite temperatures[48]. The limiting temperature for DQT is approximately the energy scale of the system J, which is formally defined below[45]. The correlation function is then evaluated via $C(t) \approx \mathrm{Re}\frac{\langle\psi_\beta|j^\epsilon(t)j^\epsilon|\psi_\beta\rangle}{L\langle\psi_\beta|\psi_\beta\rangle}$ by solving a standard differential equation problem for the temperature and the time evolution. The error of DQT scales inversely proportional to the square root of the partition function, i.e. it decreases exponentially with L. The time (temperature) evolution is performed with a $J\delta t = 0.01$ ($J\delta\beta = 0.01$) step [corresponding to an accuracy of the order of $O(10^{-8})$ in the fourth order Runge-Kutta algorithm], and up to a maximum time $t_m J = 100\pi$, giving a $\pi/t_m = 0.01J$ frequency resolution. We keep the same frequency resolution also for the ED results in the binning of the δ functions.

III. THERMAL TRANSPORT

A. Infinite temperature

Now we detail a central point of this work, i.e. the evolution of the Kitaev-Heisenberg ladder from the insulating QSL regime of the pure KL to the diffusive one of the HL close to the RSP state. To this end we present in Fig. 2 the normalized thermal conductivity $\kappa(\omega)/\Theta$, with $\Theta = \frac{\pi\beta^2}{L}\langle j^\epsilon j^\epsilon\rangle$ the sum-rule[44,49]. We distinguish two cases with respect to the pure Kitaev ladder: (a) $J_{x,y,z} = (2,1,1)J_K$, corresponding to one of its gapless phases, Fig. 2(a); (b) $J_{x,y,z} = (3,1,1)J_K$ corresponding to one of its topological gapped phases[41], Fig. 2(b). For each of the two cases, we present results for $J_H/J_K = 0.05, 0.15, 0.35, 1$ derived via DQT at $\beta = 0$ on

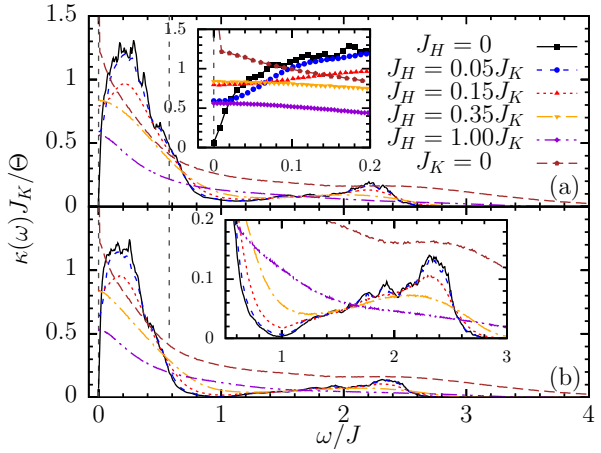

FIG. 2. Thermal conductivity versus frequency on a ladder of $L = 12$ rungs via DQT at $\beta = 0$ for: (a) $J_{x,y,z} = (2, 1, 1)J_K$ and (b) $J_{x,y,z} = (3, 1, 1)J_K$. For each case the Heisenberg couplings $J_H/J_K = 0.05, 0.15, 0.35, 1$ are considered. As a reference, the curves $J_K = 0$ and $J_H = 0$ are also shown, where the latter is obtained using ED in the fermionic representation of Eq. (2), for a chain length of $L = 32$ sites. The corresponding insets zoom into the low (a) and high frequency (b) parts of $\kappa(\omega)$.

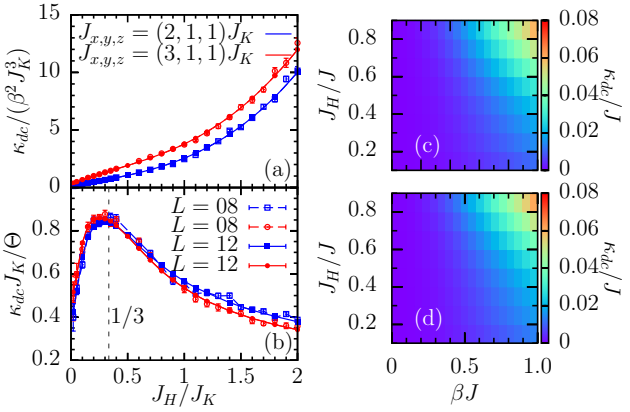

FIG. 3. (a) κ_{dc}/β^2 and (b) κ_{dc}/Θ versus the ratio J_H/J_K at $\beta = 0$ via DQT. Open points correspond to $L = 8$ while the filled ones to $L = 12$. (c) and (d), heatmap of κ_{dc} for $L = 10$ versus temperature and the couplings J_K, J_H keeping J fixed. (c) corresponds to $J_{x,y,z} = (2, 1, 1)J_K$ and (d) to $J_{x,y,z} = (3, 1, 1)J_K$.

a system of $L = 12$ rungs. As a reference, we also present results for the HL ($J_K = 0$), and for the KL ($J_H = 0$). To reduce large degeneracy effects, specific to the latter, we resort to the effective fermionic representation of Eq. (2), in that case, using chains with $L = 32$ fermionic sites and ED calculations. The frequency axes are rescaled by the "effective" coupling $J = (J_x + J_y + J_z)/3 + J_H$.

Starting with absent Heisenberg interactions, $\kappa(\omega)$ comprises two prominent structures. First, a low frequency one, which can be interpreted as the Drude weight, i.e. the quasiparticle contribution, spread over a finite frequency region due to the scattering of the itinerant fermions on the gauge disorder potential. This lifts the degeneracies of the translationally invariant system yielding a broad low frequency hump. In 1D, itinerant fermions scattering off a random (here binary) potential leads to insulating behavior[50], also for Eq. (2), i.e. $D = 0$ and $\kappa_{dc} = 0$ in the thermodynamic limit. Consequently, the correlation function exhibits a sharp low frequency dip and the maximum of $\kappa(\omega)$ is shifted away from $\omega = 0$. Second, a high frequency hump arises due to pair-breaking two-fermion contributions in j^ϵ, which survives at all temperatures–in contrast to the quasiparticle one which is suppressed at low temperatures due to the fermionic occupation factors. The two structures are continuously connected in the gapless case, while in the gapped one the correlation function vanishes for intermediate frequencies showing that the gap persists even at infinite temperatures.

Now we invoke Heisenberg coupling. This breaks the $\mathbb{Z}_2$ symmetry, renders the gauge-fluxes mobile, and restores translational invariance on some low-energy scale, expanding as J_H/J_K increases. In fact, for all $J_H \neq 0$ considered, localization breaks down, and a *finite* dc conductivity emerges in Figs. 2(a,b) and the inset of Fig. 2(a). Yet, for a substantial range of $J_H/J_K \lesssim 0.2$, and on a frequency scale of $O(1)$ the low-ω hump and depletion region persists, very suggestive of a fractionalized two component "liquid" of light(heavy) mobile Majorana fermions(gauge fluxes). Actually, the fluxes maintain a finite expectation value for $J_H \neq 0$[51]. As J_H is further increased, the system enters the Heisenberg regime, where the low-ω depletion is completely filled in and the correlation function becomes monotonous at low frequencies. Figs. 2(a,b) nicely support the naive expectation, that the coupling ratio separating the Kitaev from the Heisenberg regime should satisfy $J_H \approx J_K/3$ even if $J_x \neq J_y, J_z$, see also Fig. 3(b). Note that the artificial Drude weight depicted in the inset of Fig. 2(a) for vanishing Kitaev interactions $J_K = 0$ is an artefact of the choice of fine frequency-resolution. The established diffusive transport of a pure Heisenberg ladder[44,45] is recovered upon decreasing the frequency-resolution.

While the low-ω depletion-hump structure is intricately intertwined with the two-component nature of the fractionalization, the high-ω pair-breaking peak directly probes only one part of the fractional excitations, i.e. the two-fermion density of states. As is obvious from the inset of Fig. 2(b), this feature persists well into the range of finite Heisenberg interactions, namely $0 \leq J_H/J_K \lesssim 0.6$, thereby providing not only an unequivocal fingerprint of the original KL QSL in the presence of perturbing Heisenberg exchange, but also a measure for the crossover scale $J_H/J_K|_{rec}$, at which Majorana fermions and fluxes recombine to form triplons.

B. Finite temperatures

Let us now focus on the dc part of the thermal transport, both, versus the coupling constants, as well as the temperature and for $J_{x,y,z}/J_K = (2,1,1),(3,1,1)$, i.e. for a gapless and a gapped case. We begin with κ_{dc}/β^2 versus J_K/J_H at $\beta = 0$ in Fig. 3(a). A clearly monotonous increase with increasing J_H is observable, corroborating not only the insulating behavior of the KL, but also a *critical* coupling for localization of $J_H = 0$. In fact the data can be fitted very well by a fourth order polynomial with minor offsets, strongly suggesting an insulator as $J_H \to 0$. Next, we normalize to the sum-rule, displaying κ_{dc}/Θ in Fig. 3(b). This can be viewed as a rough measure for a zero-frequency current life-time. Once again, this figure shows a clear scale of $J_H \approx J_K/3$, separating the KL QSL from the HL RSP. The rapid decrease of κ_{dc}/Θ below this scale is dictated by the onset of localization, i.e. the vanishing of κ_{dc}. This is in sharp contrast to the physics of the HL, where the current life-time at $\beta = 0$ is a finite constant. Interestingly the two regimes are connected *non-monotonously*. It is tempting to speculate that this may imply a reduction of current scattering at the crossover to fractionalization. In passing, Figs. 3(a,b) prove that finite size effects are negligible, showing little difference between $L = 8$ and 12.

Next, we consider two contour plots of the temperature dependence of κ_{dc} versus J_H/J at $J_{x,y,z}/J_K = (2,1,1)$ and $(3,1,1)$ in Figs. 3(c) and (d). The data is represented keeping the effective energy scale J constant. This figure clearly shows how a *low-temperature* regime of enhanced dc conductivity developing in the upper right hand corner of the plot, as the system recombines localized Majorana fermions into mobile triplons upon increasing J_H/J. We note that $\kappa_{dc} \propto \beta^2$ as $\beta \to 0, \forall J_H/J$. This leads to the blue regions in Figs. 3(c,d). The main point relating to the latter is, that for $J_H = 0$ this region extends over all β, consistent with an insulator at all temperatures[35]. Finally, in view of the similar appearance of Figs. 3(c,d), differences between the gapped and gapless case, which are certainly present for $\beta > 1/J$ remain inaccessible to our numerical approach.

C. Strong rung limit

Now we change the perspective, and shed light on the impact of Kitaev exchange as a perturbation, starting from the popular strong rung limit of the HL, i.e. for $J'_H \gg J_K, J_H$. For $J_K, J_H = 0$ the ground state $|GS\rangle$ is a RSP state, with energy $E_{GS}/L = -3J'_H/4$. Finite J_K, J_H both shift E_{GS} and induce dispersive triplon excitations $|k,s\rangle$, with momentum k and magnetization s. We evaluate by perturbation theory[52–54] the one and two triplon energies,

$$\frac{\omega^{(1)}(k)}{J'_H} = 1 + \lambda \cos k, \quad \frac{\omega^{(2)}(k)}{J'_H} = 2\left(1 \pm \lambda \cos\frac{k}{2}\right), \quad (4)$$

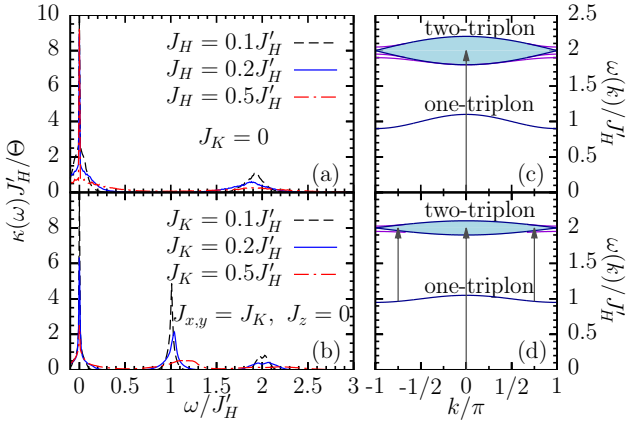

FIG. 4. (a) and (b), $\kappa(\omega)/\Theta$ versus frequency in the strong-rung limit for Heisenberg $J_H/J'_H = 0.1, 0.2, 0.5$ and Kitaev $J_K/J'_H = 0.1, 0.2, 0.5$ legs respectively obtained via ED at $\beta = 0$. (c) and (d), low lying excitation spectrum derived from perturbation theory in the strong-rung limit for Heisenberg and Kitaev legs respectively. The light blue region denotes the two-triplon continuum while the violet dashed lines two-triplon bound states.

where $\omega^{(2)}(k)$ stands for the boundaries of the two-triplon continuum, while $\lambda = J_H/J'_H$ and $J_K/2J'_H$, for Heisenberg [Fig. 4(c)] and Kitaev [Fig. 4(d)] leg interactions respectively. While these figures include our results for two-triplon bound states, they will not be considered further, since they branch off the continuum only near the zone boundary, and are not expected to contribute significantly to $\kappa(\omega)$, see Appendix A.

From Figs. 4(c,d) and Eq. (4), we can now interpret ED for $\kappa(\omega)$ with $L = 8$ at $\beta = 0$ for Heisenberg, versus Kitaev legs, in Figs. 4(a) versus (b). In both cases intensity at $\omega \sim 0$ arises from thermally populated triplon states, comprising a Drude weight on finite systems. Additionally, $j^\epsilon|GS\rangle$ generates a state in the two triplon manifold, which combined with the selection rule $\Delta k = 0$, dictated by the symmetries of the Hamiltonians, results in transitions in the range $\omega \sim 2J'_H(1 \pm \lambda)$. This is clearly seen in Figs. 4(a,b). Kitaev legs induce an additional current mode at $\omega \sim J'_H$, visible in Fig. 4(b). This qualitative difference is a direct consequence of the loss of $SU(2)$ invariance, allowing for heat-current transitions between one- and two-triplon states, which are forbidden for Heisenberg interactions due to the $\Delta S_z = 0$ selection rule. This one-triplon current intensity will feature a strong temperature dependence $\sim \exp(-J'_H/T)$ as it involves only excited states, see Fig. 6. As Figs. 4(a,b) show our interpretation remains intact up to fairly strong leg couplings $J_{K,H}/J'_H \approx 0.5$. Finally, we note that excitations to three triplon states induce low intensities, and are not considered here.

IV. SUMMARY

In conclusion, we have uncovered several fingerprints of a proximate Kitaev QSL manifested at various energy scales in the dynamical thermal transport of the Kitaev-Heisenberg ladder. While born out of a quasi-1D model study, our results should be transferable to 2D except for the singular behavior at $J_H = 0$ due to the difference between localization in 1D and 2D. We hope this may stimulate experiments, realizing that not only dc thermal conductivity is a well established experimental probe, but also dynamical heat transport can be addressed, e.g. via fluorescent flash methods[55,56] or pump-probe techniques[57]. Moreover, a "tuning" of the exchange couplings, discussed here theoretically, is also experimentally feasible - within certain limits - by chemical substitution or external pressure.

Acknowledgments.

We thank C. Hess, R. Steinigeweg, and M. Vojta, for fruitful discussions. Work of W.B. has been supported in part by the DFG through SFB 1143, project A02, and by QUANOMET and CiNNds. W.B. also acknowledges kind hospitality of the PSM, Dresden. This research was supported in part by the National Science Foundation under Grant No. NSF PHY-1748958.

Appendix A: Perturbation theory

This appendix highlights the details of the calculation presented in Sec. III C. Our starting point is the Hamiltonian of decoupled dimers

$$H_R = J'_H \sum_{i=1}^{N} \mathbf{S}_i^A \cdot \mathbf{S}_i^B \,, \tag{A1}$$

where $\mathbf{S}_i^{A,B}$ denotes spin-1/2 operators located at the i-th site of the A or B chain of the ladder, correspondingly. The eigenstates of each rung, denoted in terms of the total spin S and the total S_z component $|S, S_z\rangle$, are singlets $|0,0\rangle$ with energy $E_0^{\rm rung}/J'_H = -3/4$ and triplets $|1,0\rangle$, $|1,1\rangle$, $|1,-1\rangle$ with energy $E_1^{\rm rung}/J'_H = 1/4$. The ground state of the ladder is a direct product of spin-singlet states $|GS\rangle = \prod_{i=1}^{N} |0,0\rangle_i$, with energy $E^{\rm GS} = NE_0^{\rm rung}$, while its excitations are triplets. In the following, we consider the effect of coupling the dimers via Heisenberg or Kitaev leg interactions.

1. Heisenberg leg interactions

We first analyze the ground state and low-lying excitations in the presence of the perturbing Heisenberg Hamiltonian $H = H_R + H_H$,

$$H_H/J'_H = \lambda_H \sum_{i=1}^{N} \sum_{\alpha=A}^{B} \mathbf{S}_i^\alpha \cdot \mathbf{S}_{i+1}^\alpha \,, \tag{A2}$$

with $\lambda_H = J_H/J'_H$ the small parameter. Each bond of the perturbing Hamiltonian excites two adjacent singlets of the unperturbed ground state $|GS\rangle$ to spin-1 triplet states, while the sum of the total S_z quantum number is zero. The ground state energy up to third order in λ_H is $E_0^H/(NJ'_H) = -\frac{3}{4} - \frac{3}{8}\lambda_H^2 - \frac{3}{16}\lambda_H^3$, Ref.[53].

The first excited state of the unperturbed ladder is $3N$-fold degenerate and is obtained by promoting one rung to a triplet state $|s\rangle_n = |1,s\rangle_n \prod_{j\neq n} |0,0\rangle_j$, with $s = 0, \pm 1$. States $|s\rangle_n$ are eigenstates of H_R with energy equal to $E_0^{\rm tr} = J'_H(1 - \frac{3}{4}N)$ for any n. H_H has the effect of moving the rung excitation to nearest-neighbor rungs, thus the degeneracy is removed by constructing states with definite crystal momentum

$$|k,s\rangle = \frac{1}{\sqrt{N}} \sum_{n=1}^{N} e^{ikn} |s\rangle_n \,. \tag{A3}$$

We shall refer to states (A3) as triplons to describe a non-localized triplet excitation. The first order correction of the triplon energy is found to be equal to $E^{\rm tr}(k) = \frac{1}{J'_H}\langle k,s|H_H|k,s\rangle = \lambda_H \cos(k)$. Thus, the excitation energy of the triplons up to first order is

$$\omega_H(k) = E_0^{\rm tr} + E^{\rm tr}(k) - E^{\rm GS} = J'_H[1 + \lambda_H \cos(k)] \,. \tag{A4}$$

We note that the single triplon dispersion relation has a minimum at $k = \pm\pi$.

We now turn our attention to two-body states, namely states with total magnetization $M = \pm 2$ consisted of two-triplons with $S_z = \pm 1$ correspondingly, states with $M = \pm 1$ consisted of one triplon with $S_z = 0$ and one with $S_z = \pm 1$ and states with $M = 0$, consisted of either two triplons with $S_z = 0$ or one triplon with $S_z = 1$ and one with $S_z = -1$. First we note that since the triplon states are degenerate, the excitation energy of any two-body state with one triplon with crystal momentum k_1 and one with k_2 fall into a two-body continuum with energies $\Omega_H^{M=\pm 2}(k_1,k_2) = \omega_H(k_1) + \omega_H(k_2)$. Folding the wavevector $k = k_1 + k_2$ to the first Brillouin zone $[-\pi, \pi]$, the continuum extends between the two boundaries $\Omega_H(k)/J'_H = 2[1 \pm \lambda_H \cos(k/2)]$, expressed up to first order in λ_H. Although the two-body continuum energies are the same for any two-body state, the two-triplon bound state energy is expected to depend on the M sector. Following the calculations of Ref.[52] for the spin-1 chain based on an elementary Bethe ansatz, we find that the bound state energy of the $M = \pm 2$ sector is equal to $\Omega_H^{M=\pm 2}(k)/J'_H = 2 + \lambda_H \left[\frac{1}{2} + 2\cos(k/2)^2\right]$ which exists when $2\pi/3 \leq |k| \leq \pi$, lies above the continuum and merges with it at the cut-off momentum $2\pi/3$. Similarly for $M = \pm 1$ we find $\Omega_H^{M=\pm 1}(k)/J'_H =$

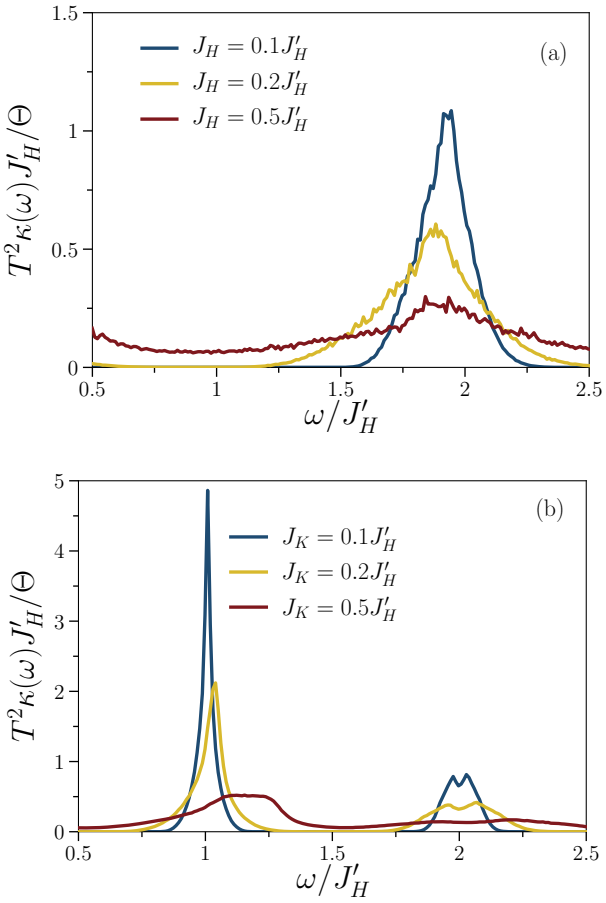

FIG. 5. High frequency part of the high temperature thermal conductivity for a Heisenberg (a) and Kitaev (b) ladder with $L = 8$ rungs for $J_H/J'_H = 0.1, 0.2, 0.5$ or $J_K/J'_H = 0.1, 0.2, 0.5$. We refer the reader to the main text of the present publication for definitions of the thermal conductivity $\kappa(\omega)$.

$2 - \lambda_H \left[\frac{1}{2} + 2\cos(k/2)^2\right]$, which lies below the continuum between wavevectors $2\pi/3 \leq |k| \leq \pi$ and finally for $M = 0$ the bound state energy is $\Omega_H^{M=0}(k)/J'_H = 2 - \lambda_H \left[1 + \cos(k/2)^2\right]$ which is stable for the whole zone $0 \leq |k| \leq \pi$. We note that in Ref.[54], analytical expressions for the bound states of sector $M = 0$ and $M = 1$ are derived based on a mapping of the model onto a Bose gas of hard-core triplets. The one- and two-particle excitation spectrum of the Heisenberg leg Hamiltonian (A2) are presented in Fig. 4(c) for $\lambda_H = 0.1$.

We note that the matrix elements $\langle n|j^\epsilon|m\rangle$ are non-vanishing for states $|n\rangle$, $|m\rangle$ that obey the selection rules $\Delta S_z = 0$ and $\Delta k = 0$. In addition, assuming that the dominant contribution in the thermal conductivity $\kappa(\omega)$ originate from the ground state $|GS\rangle_H$ to other excited states, we note that the operation $j^\epsilon|GS\rangle_H$ generates a state which belongs to the manifold of states with two excited triplons. Thus, the only possible transitions are between the ground state and the two-triplon continuum (of two $S_z = 0$ triplons or a pair of $S_z = 1$ and $S_z = -1$ triplons) at $k = 0$ which results contributions from a band of frequencies with boundary lines $\omega_\pm^H = 2J'_H(1 \pm \lambda_H)$. Figures 5(a) and (b) zoom to the higher frequency features of Figs. 4(a) and (b) respectively. A simple inspection of Fig. 5(a) reveals that in the high temperature limit most of the intensity is concentrated near the ω_-^H limit which is likely due to the fact that it involves transitions to the two-triplon continuum at its lowest gap and is thus more heavily populated. This is further confirmed by the shifting of the band to lower frequencies as the Heisenberg coupling J_H is increased. Bound states branch off the continuum near the zone boundary and are not expected to give a distinct signal in the thermal conductivity. Finally, the operation $j^\epsilon|k,s\rangle$ yields states with three excited triplons, thus we do not observe any contribution coming from transitions between single and two triplons.

2. Kitaev leg interactions

The remainder of this appendix is devoted in the analysis of the low-lying excitation spectrum in the presence of the perturbing Kitaev Hamiltonian $H = H_R + H_K$,

$$H_K/J'_H = \lambda_K \sum_{i=1}^{N/2} \left(S^x_{2i,A}S^x_{2i+1,A} + S^y_{2i,A}S^y_{2i-1,A} + S^x_{2i,B}S^x_{2i-1,B} + S^y_{2i,B}S^y_{2i+1,B}\right). \quad \text{(A5)}$$

Based on similar considerations like before we find that the ground state energy up to second order in λ_K is $E_0^K/J'_H = -\frac{3}{4}\left[N + \lambda_K^2(\frac{N}{2} - 2)\right]$. Moreover, we note that the Kitaev Hamiltonian lifts the degeneracy of the triplon modes with $S_z = \pm 1$ and the one with $S_z = 0$. More specifically, the triplon excitation energy is

$$\omega^K_{\pm 1}(k) = J'_H\left[1 + \frac{\lambda_K}{2}\cos(k)\right], \qquad \omega_0^K = J'_H, \quad \text{(A6)}$$

up to first order in λ_K. In (A6) we have omitted states that contain more than one excited rung, as is appropriate to leading order. We now turn our attention to two-triplon states, focusing first on two unbounded excitations. The boundaries of the two-body continuum consisted of any combination of two states with $S_z = \pm 1$ and wavevectors k_1 and k_2 are $\Omega_K(k)/J'_H = 2 \pm \lambda_K \cos(k/2)$, with $k = k_1 + k_2$. A two-body state consisted of two $S_z = 0$ triplons is $N(N-1)/2$ degenerate with energy $\Omega_0^K = 2J'_H$, while a two-body state consisted of one $S_z = 0$ triplon and one with $S_z = \pm 1$ triplon with crystal momentum k has an excitation energy equal to $\Omega_1^K/J'_H = 2 + \lambda_K/2\cos(k)$. In addition, the bound state energy in the $M = \pm 2$ sector is $\Omega_K^{M=\pm 2}(k)/J'_H = 2 + \frac{\lambda_K}{2}\left[\frac{1}{2} + 2\cos(k/2)^2\right]$ which exists when $2\pi/3 \leq |k| \leq \pi$ while the bound state energy of a triplon with $S_z = 1$ and one with $S_z = -1$ belonging in the $M = 0$ sector is $\Omega_K^{M=0}(k)/J'_H = 2 - \lambda_K/2\left[1 + \cos(k/2)^2\right]$. The one- and

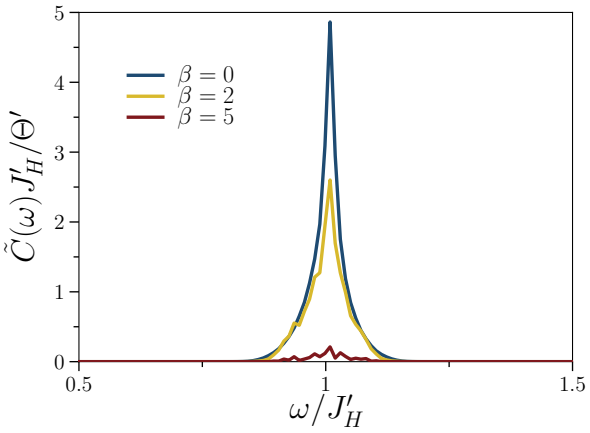

FIG. 6. Frequency dependence of the correlation function $\tilde{C}(\omega)J'_H/\Theta'$ around $\omega = 1$ of a Kitaev ladder with $L = 8$ rungs for $\lambda_K = 0.1$ and various values of the inverse temperatures β. In the low temperature limit of $\beta = 5$ we note that the dominant signal $\sim J'_H$ vanishes as expected, indicating that it originates from transitions between excited states.

two-particle excitation spectrum of the Kitaev leg Hamiltonian (A5) are presented in Fig. 4(d) for $\lambda_K = 0.1$. We note that the calculation of bound states involving triplons with $S_z = 0$ is omitted because they lie for energies in-between the bound states energies of the $M = 0$ and $M = \pm 2$ sector and are not expected to give rise to prominent signals in the $\kappa(\omega)$. Their calculation relies on an involved degenerate perturbation theory.

The selection rules between states $|n\rangle$ and $|m\rangle$ to obtain non-vanishing matrix elements $\langle n|j^\epsilon|m\rangle$ depend on the symmetries of the Hamiltonian under study. We note that for the Kitaev Hamiltonian of Eq. (A5) with less symmetries than the Heisenberg one, only the $\Delta k = 0$ rule needs to be fulfilled. As anticipated, the high-frequency part of $\kappa(\omega)$ contains contributions from the ground state to the two-particle sector from a band of frequencies with boundary lines $\omega^K_\pm/J'_H = 2 \pm \lambda_K$. The most unexpected feature of Fig. 5 is an additional dominant signal for frequencies $\sim J'_H$ which is absent for the Heisenberg perturbation scheme and originates from transitions between excited states. More precisely, the operation $j^\epsilon|k,s\rangle$ generates states in the two-triplon manifold with energies given by the two-triplon continuum as well as the two-triplon bound states. To analyze the resulting signal we need to take into account that transitions are allowed for every k in the first Brillouin zone $[-\pi, \pi]$ that will eventually produce a zoo of allowed frequencies given by the difference of the energies of the two-triplon and the single triplon states. To simplify the picture, we note that by increasing the Kitaev coupling J_K the band shifts to higher frequencies, indicating the fact that most of the intensity arises from transitions at $k = \pm\pi$ where triplons have their lowest gap and are thus more populated. At $k = \pm\pi$ the frequency band lies between the lines $\omega_1 = \Omega^{M=\pm 2}_K(\pi) - \omega^K_{\pm 1}(\pi) = J'_H(1 + 3\lambda_K/4)$ and $\omega_2 = \Omega^{M=0}_K(\pi) - \omega^K_{\pm 1}(\pi) = J'_H$.

In Fig. 6 we present the frequency dependence of the correlation function $\tilde{C}(\omega)J'_H/\Theta'$, where

$$\tilde{C}(\omega) = \mathrm{Re}\frac{1}{L}\int_{-\infty}^{\infty}\frac{d\omega}{2\pi}e^{-i\omega t}\langle j^\epsilon(t)j^\epsilon\rangle\ , \qquad \text{(A7)}$$

and the corresponding sum-rule for the correlation function $\Theta' = \frac{\pi}{L}\langle j^\epsilon j^\epsilon\rangle$. The correlation function $\tilde{C}(\omega)$ and the thermal conductivity defined in the main text are related as $\kappa(\omega) = \tilde{C}(\omega)\beta(1 - e^{-\beta\omega})/\omega$. While the latter vanishes for $\beta = 0$, the former is temperature dependent with a clear decay of its weight with decreasing temperature. The almost vanishing signal around J'_H in the low temperature limit of $\beta = 5$ is a confirmation that it involves transitions between excited states.

* a.metavitsiadis@tu-bs.de
† christina.psaroudaki@unibas.ch
‡ w.brenig@tu-bs.de

[1] L. Savary and L. Balents, Reports on Progress in Physics **80**, 016502 (2017).
[2] Y. Zhou, K. Kanoda, and T.-K. Ng, Rev. Mod. Phys. **89**, 025003 (2017).
[3] R. Coldea, D. A. Tennant, A. M. Tsvelik, and Z. Tylczynski, Phys. Rev. Lett. **86**, 1335 (2001).
[4] J. S. Helton, K. Matan, M. P. Shores, E. A. Nytko, B. M. Bartlett, Y. Yoshida, Y. Takano, A. Suslov, Y. Qiu, J.-H. Chung, D. G. Nocera, and Y. S. Lee, Phys. Rev. Lett. **98**, 107204 (2007).
[5] M. Gomilšek, M. Klanjšek, R. Žitko, M. Pregelj, F. Bert, P. Mendels, Y. Li, Q. M. Zhang, and A. Zorko, Phys. Rev. Lett. **119**, 137205 (2017).
[6] M. Hermanns, K. O'Brien, and S. Trebst, Phys. Rev. Lett. **114**, 157202 (2015).
[7] K. Le Hur, A. Soret, and F. Yang, Phys. Rev. B **96**, 205109 (2017).
[8] P. A. Lee, Journal of Physics: Conference Series **529**, 012001 (2014).
[9] A. Kitaev, Annals of Physics **321**, 2 (2006), January Special Issue.
[10] M. Hermanns, I. Kimchi, and J. Knolle, Annual Review of Condensed Matter Physics **9**, 17 (2018).
[11] L.-M. Duan, E. Demler, and M. D. Lukin, Phys. Rev. Lett. **91**, 090402 (2003).
[12] G. Jackeli and G. Khaliullin, Phys. Rev. Lett. **102**, 017205 (2009).
[13] J. c. v. Chaloupka, G. Jackeli, and G. Khaliullin, Phys. Rev. Lett. **105**, 027204 (2010).
[14] R. Yadav, N. A. Bogdanov, V. M. Katukuri, S. Nishimoto, J. van den Brink, and L. Hozoi, Scientific Reports **6**, 37925 (2016).
[15] S. K. Choi, R. Coldea, A. N. Kolmogorov, T. Lancaster,

I. I. Mazin, S. J. Blundell, P. G. Radaelli, Y. Singh, P. Gegenwart, K. R. Choi, S.-W. Cheong, P. J. Baker, C. Stock, and J. Taylor, Phys. Rev. Lett. **108**, 127204 (2012).
[16] S. Nishimoto, V. M. Katukuri, V. Yushankhai, H. Stoll, U. K. Rler, L. Hozoi, I. Rousochatzakis, and J. van den Brink, Nature Communications **7**, 10273 (2016).
[17] F. Ye, S. Chi, H. Cao, B. C. Chakoumakos, J. A. Fernandez-Baca, R. Custelcean, T. F. Qi, O. B. Korneta, and G. Cao, Phys. Rev. B **85**, 180403 (2012).
[18] K. Kitagawa, T. Takayama, Y. Matsumoto, A. Kato, R. Takano, Y. Kishimoto, S. Bette, R. Dinnebier, G. Jackeli, and H. Takagi, Nature **554**, 341 (2018).
[19] A. Banerjee, C. A. Bridges, J.-Q. Yan, A. A. Aczel, L. Li, M. B. Stone, G. E. Granroth, M. D. Lumsden, Y. Yiu, J. Knolle, S. Bhattacharjee, D. L. Kovrizhin, R. Moessner, D. A. Tennant, D. G. Mandrus, and S. E. Nagler, Nature Materials **15**, 733 (2016).
[20] L. J. Sandilands, Y. Tian, K. W. Plumb, Y.-J. Kim, and K. S. Burch, Phys. Rev. Lett. **114**, 147201 (2015).
[21] A. Glamazda, P. Lemmens, S.-H. Do, Y. S. Kwon, and K.-Y. Choi, Phys. Rev. B **95**, 174429 (2017).
[22] S. M. Winter, K. Riedl, D. Kaib, R. Coldea, and R. Valentí, Phys. Rev. Lett. **120**, 077203 (2018).
[23] J. Nasu, J. Knolle, D. Kovrizhin, Y. Motome, and R. Moessner, Nature Physics **12**, 912 (2016).
[24] S. M. Winter, K. Riedl, P. A. Maksimov, A. L. Chernyshev, A. Honecker, and R. Valentí, Nature Communications **8**, 1152 (2017).
[25] C. Hess, B. Büchner, U. Ammerahl, L. Colonescu, F. Heidrich-Meisner, W. Brenig, and A. Revcolevschi, Phys. Rev. Lett. **90**, 197002 (2003).
[26] N. Hlubek, P. Ribeiro, R. Saint-Martin, A. Revcolevschi, G. Roth, G. Behr, B. Büchner, and C. Hess, Phys. Rev. B **81**, 020405 (2010).
[27] D. Hirobe, M. Sato, Y. Shiomi, H. Tanaka, and E. Saitoh, Phys. Rev. B **95**, 241112 (2017).
[28] Y. J. Yu, Y. Xu, K. J. Ran, J. M. Ni, Y. Y. Huang, J. H. Wang, J. S. Wen, and S. Y. Li, Phys. Rev. Lett. **120**, 067202 (2018).
[29] R. Hentrich, A. U. B. Wolter, X. Zotos, W. Brenig, D. Nowak, A. Isaeva, T. Doert, A. Banerjee, P. Lampen-Kelley, D. G. Mandrus, S. E. Nagler, J. Sears, Y.-J. Kim, B. Büchner, and C. Hess, Phys. Rev. Lett. **120**, 117204 (2018).
[30] I. A. Leahy, C. A. Pocs, P. E. Siegfried, D. Graf, S.-H. Do, K.-Y. Choi, B. Normand, and M. Lee, Phys. Rev. Lett. **118**, 187203 (2017).
[31] R. Hentrich, M. Roslova, A. Isaeva, T. Doert, W. Brenig, B. Büchner, and C. Hess, ArXiv e-prints (2018), arXiv:1803.08162 [cond-mat.str-el].
[32] S.-H. Baek, S.-H. Do, K.-Y. Choi, Y. S. Kwon, A. U. B. Wolter, S. Nishimoto, J. van den Brink, and B. Büchner, Phys. Rev. Lett. **119**, 037201 (2017).
[33] Y. Kasahara, T. Ohnishi, Y. Mizukami, O. Tanaka, S. Ma, K. Sugii, N. Kurita, H. Tanaka, J. Nasu, Y. Motome, T. Shibauchi, and Y. Matsuda, ArXiv e-prints (2018), arXiv:1805.05022 [cond-mat.str-el].
[34] J. Nasu, J. Yoshitake, and Y. Motome, Phys. Rev. Lett. **119**, 127204 (2017).
[35] A. Metavitsiadis and W. Brenig, Phys. Rev. B **96**, 041115 (2017).
[36] A. Metavitsiadis, A. Pidatella, and W. Brenig, Phys. Rev. B **96**, 205121 (2017).
[37] A. K. R. Briffa and X. Zotos, Phys. Rev. B **97**, 064406 (2018)
.
[38] G. L. Stamokostas, P. E. Lapas, and G. A. Fiete, Phys. Rev. B **95**, 064410 (2017)
.
[39] B. Dalla Piazza, M. Mourigal, N. B. Christensen, G. J. Nilsen, P. Tregenna-Piggott, T. G. Perring, M. Enderle, D. F. McMorrow, D. A. Ivanov, H. M. Rønnow, Nature Physics **11**, 62 (2015).
[40] M. Gohlke, R. Verresen, and R. Moessner, and F. Pollmann, Phys. Rev. Lett. **119**, 157203 (2017).
[41] X.-Y. Feng, G.-M. Zhang, and T. Xiang, Phys. Rev. Lett. **98**, 087204 (2007).
[42] N. Wu, Physics Letters A **376**, 3530 (2012).
[43] E. Dagotto and T. M. Rice, Science **271**, 618 (1996).
[44] X. Zotos, Phys. Rev. Lett. **92**, 067202 (2004).
[45] R. Steinigeweg, J. Herbrych, X. Zotos, and W. Brenig, Phys. Rev. Lett. **116**, 017202 (2016).
[46] G. D. Mahan, *Many-particle physics* (Plenum Press, New York, 1981) pp. xiv, 1003.
[47] X. Zotos and P. Prelovšek, Phys. Rev. B **53**, 983 (1996).
[48] R. Steinigeweg, J. Gemmer, and W. Brenig, Phys. Rev. Lett. **112**, 120601 (2014).
[49] B. S. Shastry, Phys. Rev. B **73**, 085117 (2006).
[50] P. W. Anderson, Phys. Rev. **109**, 1492 (1958).
[51] C. E. Agrapidis, J. van den Brink, and S. Nishimoto, (unpublished).
[52] N. Papanicolaou and P. Spathis, Journal of Physics: Condensed Matter **2**, 6575 (1990).
[53] M. Reigrotzki, H. Tsunetsugu, and T. M. Rice, Journal of Physics: Condensed Matter **6**, 9235 (1994).
[54] V. N. Kotov, O. P. Sushkov, and R. Eder, Phys. Rev. B **59**, 6266 (1999).
[55] M. Montagnese, M. Otter, X. Zotos, D. A. Fishman, N. Hlubek, O. Mityashkin, C. Hess, R. Saint-Martin, S. Singh, A. Revcolevschi, and P. H. M. van Loosdrecht, Phys. Rev. Lett. **110**, 147206 (2013).
[56] M. Otter, V. Krasnikov, D. Fishman, M. Pshenichnikov, R. Saint-Martin, A. Revcolevschi, and P. van Loosdrecht, Journal of Magnetism and Magnetic Materials **321**, 796 (2009), proceedings of the Forth Moscow International Symposium on Magnetism.
[57] A. Schmidt, M. Chiesa, X. Chen, and G. Chen, Review of Scientific Instruments **79**, 064902 (2008).